Experimental and theoretical study of the Raman spectrum in KTa$_{1-x}$Nb$_x$O$_3$ solid solutions

G. E. Kugel, H. Mesli, and M. D. Fontana

Centre Lorrain d'Optique et d'Electronique du Solide, Ecole Supérieure d'Electricité,
2 rue Edouard Belin, 57078 Metz, Cedex 03 France

D. Rytz

Hughes Research Laboratories, Malibu, California 90265
(Received 5 February 1987; revised manuscript received 19 October 1987)

The three symmetry components of the Raman spectra in paraelectric KTa$_{1-x}$Nb$_x$O$_3$ (KTN) mixed crystals have been measured as a function of temperature ($T_c < T < 800$ K) and for several niobium concentrations ($x=0.008$, $x=0.012$, $x=0.02$, $x=0.09$, $x=0.21$, and $x=0.36$). The results are analyzed in the framework of an extended shell model by assuming an anisotropic and nonlinear polarizability of the oxygen ion. This intraionic anharmonicity is indicated to be primarily responsible for the strong second-order Raman effect. Conclusions on the leading mechanism of the phase transitions in the KTN system are discussed.

I. INTRODUCTION

The use of the Raman light-scattering spectroscopy to study the dynamical aspects connected to structural phase transitions (SPT's) in ferroelectric and related crystals has been extensively carried out in the last few decades.[1-3] Indeed Raman spectroscopy provides valuable information on both the static and dynamic microscopic phenomena accompanying reversible SPT's, which can complete useful data obtained by other techniques such as infrared spectroscopy, neutron, x-ray or Brillouin scattering, elastic, dielectric, refractive index, or birefringence measurements.

In the present work, Raman scattering has been used in order to investigate the mechanism leading to a SPT and the characteristics of the impurity-induced transitions in potassium tantalate-niobate mixed crystals of the formula KTa$_{1-x}$Nb$_x$O$_3$ (KTN) for various niobium concentrations. In this paper we restrict our interest to the study of the paraelectric cubic phase only.

Pure KTaO$_3$ remains paraelectric down to 0 K, although it exhibits an exemplary soft mode, the frequency of which goes from 80 cm^{-1} at room temperature down to a value of 1.5 cm^{-1}, with a slight stabilization at low temperature by quantum fluctuation effects.[4,5] The introduction in KTaO$_3$ of even small concentrations of impurities, for instance, replacing Ta ions by Nb ions, induces a ferroelectric phase. The transition temperature T_c can be adjusted between -273 and 430 °C by choosing an appropriate niobium concentration.[5-7] Much theoretical and experimental work has been recently devoted to the influence of these impurities on phenomena coupled to the phase transition (temperature dependence of the soft mode, occurrence of a central peak) and to the mechanisms drastically modifying the crystal bulk properties.[7-11]

The question which is still seriously debated is whether the low-temperature polar phase originates from spontaneous collective displacements of the ions below T_c (displacive SPT) or from the freezing of the impurity-induced dipolar motion (dipolar spin-glass SPT). From the pressure-induced low-frequency dispersion of the dielectric susceptibility and the vanishing of the dielectric anomalies with dc biasing field, Samara[12] suggested that the niobium ion occupies an "off-center" position at atmospheric pressure and at high temperature ($T > T_c$), implying a glasslike behavior without long-range ordering. Kleemann et al.[13] interpreted their birefringence and refractive index data in terms of a "cooperative dipole glass model" which assumes local transitions of impurity clusters followed by a strain-induced collective ordering of these clusters, finally yielding a long-range order. These two models are based on the idea that the Nb ions behave as Ising-type impurity centers, which have been classified by Halperin-and Varma[14] as "frozen" or "slowly relaxing" defects. An alternative description is provided by Prater et al.,[15] who analyzed their Raman spectroscopy data on KTN with dilute niobium concentrations in terms of impurity of class B_3. The niobium ions occupy symmetric sites which favor the low-temperature phase only weakly in the sense that any local departure from the symmetric phase occurs on a time scale of the order of the TO phonon period. Intermediate and complementary pictures have been given by other authors.[11,16] Yacoby[16] studied the Raman spectrum of a KTN crystal with a 6% niobium concentration and concluded that the individual niobium centers induce fluctuations or microdistorsions in the paraelectric phase of a KTaO$_3$ host crystal, whose amplitudes decrease with increasing temperatures above T_c. Lee et al.[11] analyzed their critical quasielastic light scattering on KTN samples with low niobium concentrations in terms of disorder-induced fluctuations of the polarizabilities and

force constants.

More recently, Lyons et al.,[17] by combining results of inelastic light scattering with earlier dielectric relaxation data, found clear evidence for a cooperative dynamic regime, suggesting, for the crystal with $x = 0.009$, a transition to a glassy state at 3 K. The mechanism of the transition is the following: (i) the niobium ions are on site at high temperature; (ii) their off-site position residence time increases with lowering temperature; (iii) dipolar clusters with Nb residing along [111] and with strongly increasing relaxation times (obeying a Vogel-Fulcher law) are formed.

All the above considerations on the nature of the SPT's in KTN are concerned with physical mechanisms which play a direct and dominant role in the near vicinity of T_c and which are initiated by different couplings providing the conditions of crystal instability. In the present paper we focus on these first interactions, which are treated in terms of an intraionic anharmonicity of the oxygen ion responsible for the lowest-frequency mode softening. Furthermore, we discuss how the introduction of niobium ions in the host $KTaO_3$ lattice modifies these primary couplings. The present work reports a detailed experimental and theoretical analysis of the Raman spectrum in the paraelectric phase where first-order Raman scattering is forbidden by symmetry. The eventual occurrence of defect-induced first-order lines is studied as a function of temperature and niobium concentration within the glasslike behavior model. In addition, the strong scattered intensity is demonstrated to be due to second-order processes related to the anharmonic couplings.

Having in mind these various features, we re-examine experimentally the Raman spectrum of KTN samples with both low ($x = 0.008$, $x = 0.012$, and $x = 0.02$) and high ($x = 0.09$, $x = 0.21$, and $x = 0.36$) niobium concentration. The investigations have been performed in a wide temperature range, extending from $T \cong 800$ K to temperature in the vicinity of T_c (but with $T > T_c$), and for frequencies up to 1600 cm^{-1}. Our Raman results are discussed in light of other recently available data, such as the dependence of the soft mode,[9,18] and more generally of the phonon dispersion curves, on temperature, and niobium concentration.[19–21] These are performed in the framework of dynamical model calculations, allowing computation of the one- and two-phonon densities of states as well as of the second-order Raman spectrum.[22,23]

The present paper is organized as follows. In Sec. II we present the experimental methods and the Raman results obtained on dilute Nb-concentration crystals ($x \leq 0.02$) on one hand, and higher Nb-concentration crystals up to $x = 0.36$ on the other hand. In Sec. III we briefly report the physical ideas underlying the anharmonic dynamical model which interprets the softening of the ferroelectric vibration modes and enables the calculation of the second-order Raman spectrum (the procedure of which is given). In Sec. IV we compare the experimental data with the theoretical results and discuss the most relevant features appearing in the cubic phase on the basis of the considerations given in the beginning of the present section.

II. EXPERIMENTAL METHODS AND RESULTS

A. Experimental techniques and samples

The Raman scattering spectrometer employed in the present work consists of a Spectra-Physics helium-neon laser as the excitation source (6328 Å) and a Spex double monochromator for dispersion with a photon-counting readout system using a cooled RCA C31034 phototube for detection. The system is linked with a Datamate microprocessed controller and acquisition processor, the data being stored on a floppy disk. The KTN samples have been cooled from room temperature to low temperature ($T = 10$ K) with an Air-Product Displex cryostat driven by an automatic temperature indicator controller. For the measurements between room and high temperature, the samples have been mounted in a temperature-controlled furnace, the temperature being detected by a Chromel-Alumel thermocouple located near the sample. The whole system was arranged in the conventional 90° scattering geometry.

The Raman scattering measurements have been performed on six crystals of $KTa_{1-x}Nb_xO_3$, with $x = 0.008$, $x = 0.012$, $x = 0.02$, $x = 0.09$, $x = 0.21$, and $x = 0.36$. The samples used were rectangular-shaped plates approximately $9 \times 1 \times 0.7$ mm^3 for the three dilute Nb concentration crystals, $6 \times 1 \times 0.5$ mm^3 for $x = 0.09$, and $5 \times 5 \times 5$ mm^3 for $x = 0.21$ and $x = 0.36$. For the various crystals, the faces of the plates were cut parallel to the (100) planes. The crystal with $x = 0.02$ was available with supplementary faces parallel to (011) and (111) planes. These samples were cut from larger crystals grown by a flux method described elsewhere.[24] They exhibited a small gradient of concentration along the z axis of about 0.002 mol/mm, which may lead to a slight distribution of the transition temperature T_c across the sample. The values of the T_c's have been determined by ultrasonic and dielectric methods[8] to be 0 K for $x = 0.008$ 17.6 K for $x = 0.012$, 28 K for $x = 0.02$, 93 K for $x = 0.09$, 175 K for $x = 0.21$, and 275 K for $x = 0.36$. Recent second-harmonic generation[9] (SHG) and linear birefringence (LB) determination[13] on the same samples yields the following T_c's: for $x = 0.008$, $T_c = 0$ K by SHG and 10 K by LB; for $x = 0.012$, $T_c = 21$ K by SHG and 17 K by LB; for $x = 0.02$, $T_c = 31$ K by SHG and 31.5 K by LB.

The discrepancies (strong for the crystal with $x = 0.008$) in the T_c's observed in the crystals with the same nominal concentration are due mainly to the broad smearing out of both the SHG and LB intensities, leading to difficulties in the choice of an exact T_c. Furthermore the samples originate from a large single crystal and were sometimes cut far apart from each other and thus may have noticeably different concentrations.

B. Experimental results

In the report of the experimental data we distinguish the Raman measurements concerning dilute KTN crystals ($x \leq 0.02$) from those concerning higher niobium

concentration crystals ($x \geq 0.09$). This is justified by the fact that the sequences of SPT's are different for these limiting cases. For $x \leq 0.02$, only a cubic-rhombohedral transition, whose nature is still largely debated, occurs. For the crystals with higher niobium concentration, the SPT's sequence cubic-tetragonal-orthorhombic-rhombohedral takes place and the mechanism of the transitions seems to be of different nature.[5,25]

1. Raman spectra for low Nb concentration crystals ($x \leq 0.02$)

In Fig. 1 we report the Raman spectra at room temperature on the three KTN crystals, with $x = 0.008$, $x = 0.012$, and $x = 0.02$. The 90° scattering geometry has been used with the laser beam along the (001)axis and without analysis of the scattered light. The major feature observed in the Raman spectra of the three crystals is the appearance of the same structures at the same energy as in pure $KTaO_3$.[26] The lines have been analyzed in detail in $KTaO_3$ as being due to second-order Raman scattering by pairs of phonons at the Van Hove critical points.

In accordance with the analysis of Nielsen and Skinner[26] and of Migoni et al.,[27,28] the main structure noted S_1 to S_9 can be attributed to the scattering processes reported in Table I.

Recently measured phonon dispersion curves in pure $KTaO_3$ ascertain the fact that the critical-zone boundary point, which is involved in the second-order scattering process, is the X point.[19] Some weak shoulders S'_1 to S'_4 appear at 213, 328, 380, and 430 cm^{-1}. The introduction of small amounts of niobium in the pure $KTaO_3$ does not lead to any significant modification in the room-temperature Raman spectra. Only a very broad quasi-elastic background, which has already been observed by Prater et al.[15] appears with increasing Nb concentration. By Raman scattering on the KTN crystal with 6% Nb, Yacoby[16] identified some lines at 184, 200, 280, and 546 cm^{-1} as due to scattering from the first-order lines LO_1, TO_2, TO_3, and TO_4. In our experiments, structures are detected in the intermediate region between 150 and 300 cm^{-1} which could correspond to the lines identified by Yacoby. Nevertheless, we will see that even for higher niobium concentration (up to $x = 0.36$), and due to the
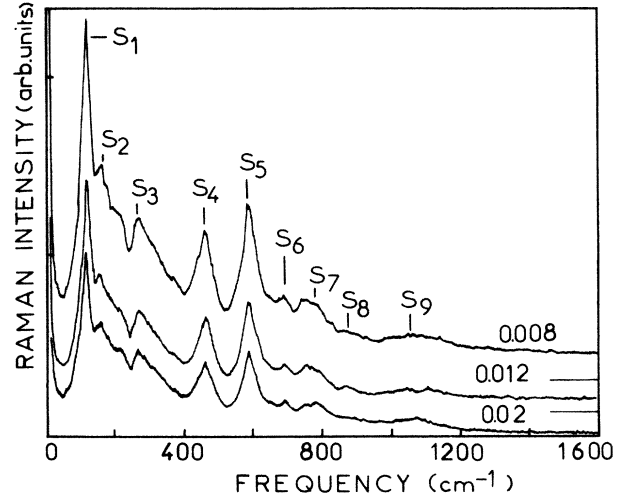

FIG. 1. Raman spectra at room temperature measured in the three $KTa_{1-x}Nb_xO_3$ crystals with $x = 0.008$, $x = 0.012$, and $x = 0.02$.

difficulty in substracting the signal from the background, the dependence of the line intensities with defect concentration is not easy to evaluate.

A further major feature in the Raman scattering spectra concerns the relative intensities of the scattered light with respect to the scattering configuration, and consequently to the symmetry component of the spectrum. It is known that in a cubic material, the symmetry Raman tensor has only three independent components which correspond to the irreducible components $A_{1g}(\Gamma_1)$, $T_{2g}(\Gamma'_{25})$, and $E_g(\Gamma_{12})$ of a second-rank tensor. The components have been measured systematically on the KTN crystal with $x = 0.02$ where samples with faces parallel to a (001) plane and to a (110) plane were available. Figure 2 represents the Raman spectra which have been recorded at room temperature with the following scattering configurations: $Z(XX)Y$, $Z(XZ)Y$, and $XY(X\overline{Y},XY)Z$, which have been shown to correspond, respectively, to the following combinations of irreducible components: $A_{1g} + 4E_g$, T_{2g}, and $3E_g$ (X, Y, and Z are the cubic axes). One important point to observe in the scattering profiles

TABLE I. Phonon energy assignments for the second-order Raman spectra and derived one-phonon energies at room temperature.

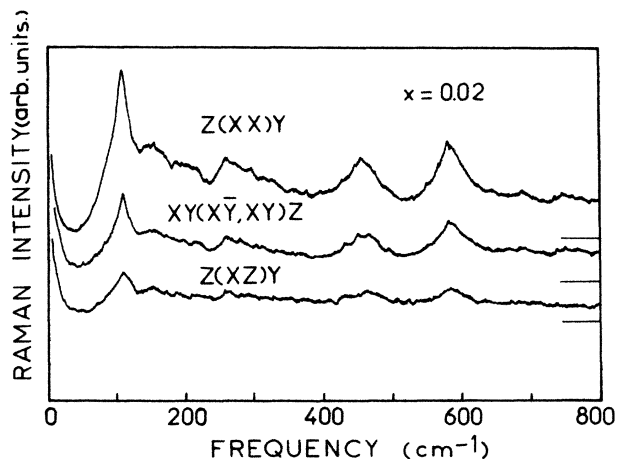| Peak	Second-order Raman Energy (cm^{-1})	Assignment	One-phonon energy Assignment	Energy (cm^{-1})
$S1$	119	$2TA(X)$	$TA(X)$	≈ 60
$S2$	160	$TO2(X) - TA(X)$	$TO2(X)$	≈ 220
$S3$	272	$TO2(X) + TA(X)$		
$S4$	460	$TO3(X) - TA(X)$	$TO3(X)$	≈ 520
$S5$	584	$TO3(X) + TA(X)$	$TO1(X)$	≈ 180
$S6$	695	$TO3(X) + TO1(X)$		
$S7$	763	$TO3(X) + TO2(X)$		
$S8$	875	$2LO2(X, \Gamma)$	$LO2(X, \Gamma)$	≈ 440
$S9$	1093	$2TO3(\Gamma)$	$TO3(\Gamma)$	≈ 550

FIG. 2. Room-temperature Raman scattering in $KTa_{1-x}Nb_xO_3$ for $x = 0.02$ with different scattering configurations.

FIG. 4. Dependence with temperature of the Raman spectrum in $KTa_{1-x}Nb_xO_3$ with $x = 0.012$.

is that the same structures appear in the various symmetry components. Nevertheless, it is obvious that the most important contribution to the spectrum originates from the A_{1g} symmetry, while the components E_g and, particularly, T_{2g} are of much weaker intensity. The same behavior has been observed in $KTaO_3$ (Ref. 26) and $SrTiO_3$,[29] as well as in alkaline-earth oxides with NaCl structure.[30]

Figures 3, 4, and 5 represent the behavior as a function of temperature of the Raman spectra for the KTN samples containing 0.8%, 1.2%, and 2% niobium, respectively. In the high-temperature range $(T > 300$ K), the dependence in energy of the previous structures S_1 to S_9 is coherent with the neutron scattering results of Currat et al.[19] on $KTaO_3$. The influence of niobium introduction is negligible. Furthermore, the scattered intensity of the various structures shows a temperature dependence
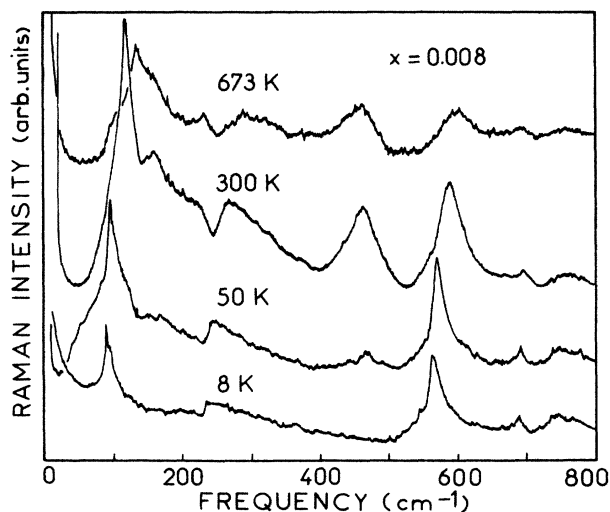
in accordance with the second-order scattering temperature factors. This observation applies to the spectra corresponding to the low-temperature range $(T_c < T < 300$ K) and distinguishes the nature of the combination band which is involved in the scattered structures. As shown in Sec. III, second-order sum bands depend on a phonon occupation number such as $(n_{j1} + n_{j2} + n_{j1}n_{j2} + 1)$, where n_j is the Bose-Einstein thermal factor for the mode j, whereas the difference-bands intensity varies as $(n_{j1}n_{j2} + n_{j2})$. For this last case, the intensity approaches zero as the temperature is reduced. This fact is clearly seen by the disappearance at low temperatures of the structures S_2 (160 cm^{-1}) and S_4 (460 cm^{-1}), which have been rightfully assigned as difference-processes bands.

A last interesting feature, which appears in the low-temperature spectra, concerns the evidence, on the low-frequency side of the 2TA(X) peak, of a broad shoulder.
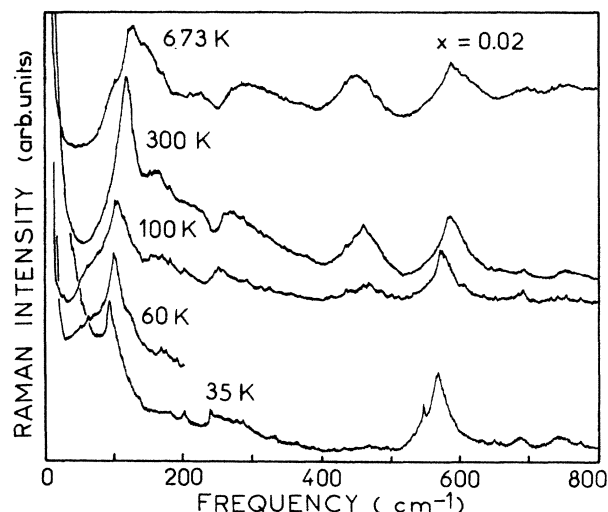

FIG. 3. Dependence with temperature of the Raman spectrum in $KTa_{1-x}Nb_xO_3$ with $x = 0.008$.

FIG. 5. Dependence with temperature of the Raman spectrum of $KTa_{1-x}Nb_xO_3$ with $x = 0.02$.

This structure moves down in frequency with temperature decreasing towards T_c and seems to be enhanced by the increase of the niobium concentration. Similar features have been observed by Prater et al.[15] who attributed it either to further two-phonon scattering or to a manifestation of an impurity-induced scattering from the TO_1 ferroelectric phonon mode. Since the temperature dependence of the soft mode is now perfectly known within the cubic phase by our recent hyper-Raman measurements,[9] we can discard the last assumption. We rather believe in a second-order scattering which necessarily involves the temperature dependent TO_1 mode. The position in frequency of the shoulder and its temperature-dependence supports, in the three investigated samples, its second-order nature. The diffuse broadness of the structure may be explained by the strong damping of the TO_1 mode occurring near T_c, as evidenced by the hyper-Raman scattering.

2. Experimental spectra for x = 0.09, x = 0.21, and x = 0.36

The room-temperature Raman spectra recorded for KTN crystals with larger amounts of niobium ($x = 0.09$, $x = 0.21$, and $x = 0.36$) are reported in Fig. 6. The various bands S_1 to S_7 already observed in $KTaO_3$, as well as in the KTN samples, with low niobium concentration are still present at nearly the same frequencies. Nevertheless the scattering profile is revealed to be more diffuse and enlarged with increasing niobium concentration.

The structures near 200 cm^{-1}, which have been assigned by several authors[15,16] to be due to first-order scattering induced by niobium, are still detected with an intensity which seems not to be proportional to the Nb concentration. The difficulty to extract these lines from the strong background makes it difficult to make a corre-

lation between the niobium concentration and their scattered intensity.

III. THEORETICAL CONSIDERATIONS

A. The dynamical model

The two-phonon Raman effect in crystals is understood in terms of theoretical calculations of the thermally weighted two-phonon density of states multiplied by the second-order coefficients issued from the expansion of the polarizability tensor with normal coordinates.[31] It has been shown by Bruce and Cowley[32] that these coefficients can be obtained by considering nonlinear intraionic interactions within a shell-model formalism. Consequently, the calculation of a second-order Raman spectrum requires a dynamical model which gives a detailed description of the phonon dispersion curves $\omega(q,j)$ and which also provides a possibility of calculating the $P_{\alpha\beta}(\genfrac{}{}{0pt}{}{q}{j_1}\ \genfrac{}{}{0pt}{}{-q}{j_2})$ coefficients appearing in the expansion of the polarizability tensor.

The essential problem in these calculations is to postulate on the origin of the nonlinearity in the model. In our case we assume a nonlinear electron-ion coupling in the most polarizable ion: i.e., the oxygen ion. The importance of such an intraionic anharmonicity in ionic crystals has been shown in the investigation of Raman spectra of alkaline-earth oxides (CaO,SrO) by Haberkorn et al.[33] and Bilz et al.[34] Furthermore, Migoni et al.[27,28] demonstrated in the framework of a fourth-order core-shell interaction inside the O^{2-} ion that this nonlinearity is responsible for the ferroelectric mode softening and also for the strong second-order Raman spectra in $KTaO_3$ and $SrTiO_3$. In the present paper we aim to extrapolate this model to Raman calculations in the mixed KTN solid solutions as function of temperature and niobium concentration.

The dynamical model used here[22,23] is a modified version of the shell model of Cowley[35] and Stirling,[36] in which the harmonic core-shell constant of the oxygen ion (k_O) is substituted by a tensor with only two nonzero parameters k_{O-A} and k_{O-B}. These quantities are the corresponding coupling constants in the direction of the neighboring A(K) and B(Ta or Nb) ions, respectively. This anisotropy originates from the introduction in the expansion in terms of relative shell displacements of the potential in the B ion direction of a nonlinear fourth-order contribution k_4^{O-B} in addition to the normal linear k_2^{O-B} term. In the self-consistent phonon approximation, these assumptions lead to a temperature-dependent $k_{O-B}(T)$ core-shell interaction which can be expressed as

$$k_{O-B}(T) = k_2^{O-B} + \tfrac{1}{2}k_4^{O-B}\langle W_{O-B}^2 \rangle_T \ . \tag{1}$$

The quantity $\langle W_{O-B} \rangle_T$ is the thermal average of the oxygen shell displacements in the B ion direction, which is calculated by using the oxygen shell eigenvectors f obtained from the shell model. Since this paper is focused on the Raman calculations, the authors advise the
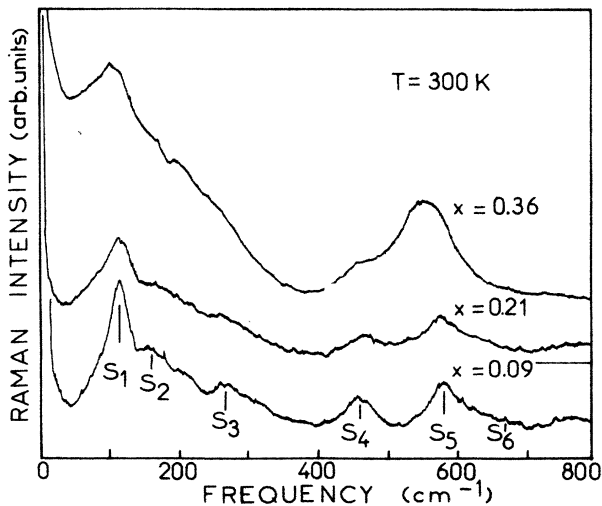

FIG. 6. Room temperature Raman spectra in $KTa_{1-x}Nb_xO_3$ with high concentrations of niobium ($x = 0.09$, $x = 0.21$, and $x = 0.36$).

readers to refer to their previous paper on the soft mode and lattice dynamical calculations on the KTN system, in which the computing procedure and the deduced results are analyzed in detail.[22,23]

B. Raman scattering intensity calculations

As previously mentioned, the second-order Raman intensity can be expressed as

$$I^{(2)}_{\alpha\beta\gamma}\delta(\omega)=\sum_{q,j_1 j_2} P_{\alpha\beta}\begin{bmatrix} q & -q \\ j_1 & j_2 \end{bmatrix} P_{\gamma\delta}\begin{bmatrix} q & -q \\ j_1 & j_2 \end{bmatrix}\rho(\omega,q,j_1,j_2) \ . \tag{2}$$

The expression $\rho(\omega,q,j_1,j_2)$ is the thermally weighted two-phonon density of states,

$$\rho(\omega,q,j_1,j_2)=[n(q,j_1)+1][n(-q,j_2)+1)]\delta[\omega-\omega(q,j_1)-\omega(-q,j_2)]$$

$$+[n(q,j_1)+1]n(-q,j_2)\delta[\omega-\omega(q,j_1)+\omega(-q,j_2)]$$

$$+n(q,j_1)[n(-q,j_2)+1]\delta[\omega-\omega(q,j_1)-\omega(-q,j_2)]$$

$$+n(q,j_1)n(-q,j_2)\delta[\omega+\omega(q,j_1)+\omega(-q,j_2)] \ , \tag{3}$$

$n(q,j)$ is the usual phonon occupation number of mode j.

Migoni[37] has shown that the second-order coefficient $P_{\alpha\beta}\begin{smallmatrix} q & -q \\ j_1 & j_2 \end{smallmatrix}$ for the three irreducible components A_{1g}, E_g, and T_{2g} can be calculated as quadratic forms of the core-shell interactions weighted by expressions involving the eigenvectors $f(q,j)$ of the oxygen shell displacements. Since in our case, only the parameter k_4^{O-B} is considered different from zero, the $P_{\alpha\beta}\begin{smallmatrix} q & -q \\ j_1 & j_2 \end{smallmatrix}$ are simplified such as

$$P_{\alpha\beta}(A_{1g})\begin{bmatrix} q & -q \\ j_1 & j_2 \end{bmatrix}=\alpha k_4^{O-B}\eta^2_{O-B}\left[f_\alpha\begin{bmatrix} q \\ O_\alpha, j_1 \end{bmatrix}f_\alpha\begin{bmatrix} -q \\ O_\alpha, j_2 \end{bmatrix}\right] , \tag{4}$$

$$P_{\alpha\beta}(E_g)\begin{bmatrix} q & -q \\ j_1 & j_2 \end{bmatrix}=\alpha k_4^{O-B}\eta^2_{O-B}\left[f_\alpha\begin{bmatrix} q \\ O_\alpha, j_1 \end{bmatrix}f_\alpha\begin{bmatrix} -q \\ O_\alpha, j_2 \end{bmatrix}-f_\beta\begin{bmatrix} q \\ O_\beta, j_1 \end{bmatrix}f_\beta\begin{bmatrix} -q \\ O_\beta, j_2 \end{bmatrix}\right] , \tag{5}$$

$$P_{\alpha\beta}(T_{2g})\begin{bmatrix} q & -q \\ j_1 & j_2 \end{bmatrix}=0 \ . \tag{6}$$

The $f_\alpha(O_\beta,{}^q_j)$ is the α component of the shell eigenvector of the oxygen ion located along the β direction for the j mode. The quantity η^2_{O-B} is expressed from the shell model matrix elements S and Y such as

$$\eta_{O-B}=\sum_{K'}S^{-1}_{\alpha\alpha}\begin{bmatrix} O \\ K & K' \end{bmatrix}Y_{K'} \ .$$

The general expression of the $P_{\alpha\beta}$ coefficients as functions of all the core-shell tensor elements can be found in Ref. 37.

Let us now describe the procedure used in our calculations: (a) research, for each niobium concentration x and for each temperature T of the $k_{O-B}(T)$ value giving to the soft-mode frequency as obtained by the lattice dynamical model calculation in accordance with the experimental data; (b) calculation, within the self-consistent procedure, of the thermal average of the oxygen shell displacements in the B ion direction $\langle W^2_{O-B}\rangle T$ and deduction for each Nb concentration x, of the k_2^{O-B} and k_4^{O-B} parameters [Eq. (1)]; (c) determination, for each x and T values, of the phonon dispersion curves $\omega(q,j)$ in the entire Brillouin zone and of the corresponding core $e(q,j)$ and shell $f(q,j)$ eigenvectors.

(d) calculation, by use of the $\omega(q,j)$ values, of the thermally weighted phonon density of states as given in Eq. (3) for the second-order scattering. (the one-phonon frequency distribution has also been calculated); (e) calculation of the polarizability element $P_{\alpha\beta}$ as expressed in Eq. (4)–(6); (f) calculation of the second-order Raman intensity [Eq. (2)] for the two relevant components A_{1g} and E_g of the irreducible representation for each Nb concentration x and as a function of temperature.

The main results of these calculations will be given and analyzed in Sec. IV.

IV. RESULTS OF THE CALCULATIONS AND DISCUSSIONS

A. Results of the model calculation

The first step of the calculations concerns the determination of the model parameters which explain the temperature dependence of the mode frequencies. Since this paper is mainly focused on the Raman results, the reader is advised to refer to Ref. 22 and 23 for a detailed analysis of the dynamical aspect. As typical results, we compare in Fig. 7 the experimental and theoretical behavior of the
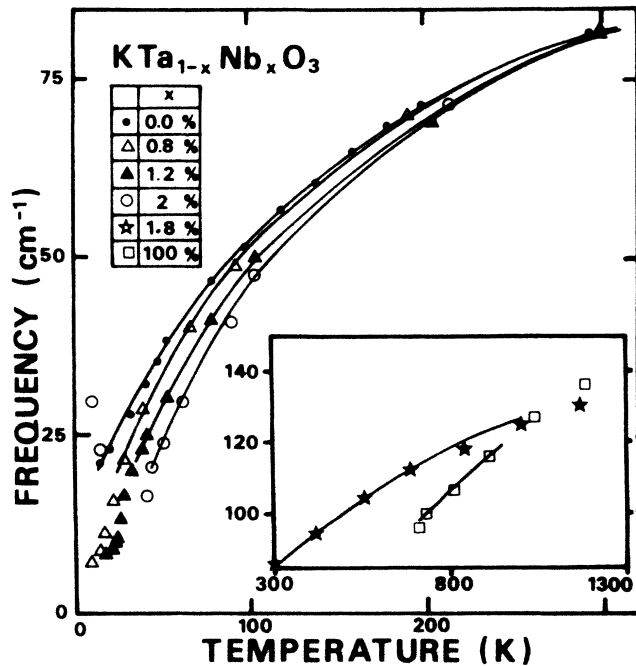
FIG. 7. Ferroelectric soft-mode frequency in the $KTa_{1-x}Nb_xO_3$ system as a function of temperature. The data between 0 and 300 K are hyper-Raman results, those between 300 and 1300 K are IR results.

ferroelectric mode temperature dependence for various niobium concentrations. This nontrivial agreement, issued from a self-consistent model calculation, indicates that the softening of the ferroelectric mode originates from the anisotropic and nonlinear polarizability of the oxygen ion, the magnitude of which is increased with increasing Nb concentration. In Fig. 8 the phonon dispersion curves of KTN ($x = 0.02$) calculated at room temperature are shown. Such calculations have been performed systematically for additional solid solutions of KTN in a large temperature range. The results will by analyzed and compared with recent neutron scattering data in a forthcoming paper.
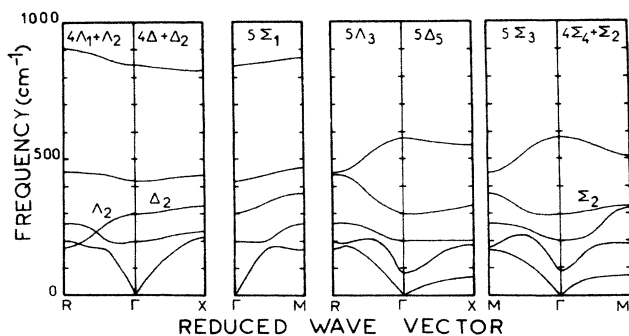

FIG. 8. Phonon dispersion curves of $KTa_{1-x}Nb_xO_3$ ($x = 0.02$) at room temperature in the three high-symmetry directions.

B. Comparison between the Raman spectra and the phonon density of states

As mentioned in Sec. I, the appearance of first-order lines in a cubic crystal containing impurities can be explained either from impurity-induced Raman scattering such as local or resonant modes, or from the disorder which is inherent to mixed crystals. In the last case the scattering is proportional to the first-order phonon frequency distribution. This function has been calculated for each KTN crystal and as a function of temperature by using a channel of 8 cm^{-1} and by sampling more than 1000 points of the irreducible 1/48 of the Brillouin zone. An example compiling the room-temperature results of the calculation is reported in Fig. 9 for the KTN crystal with $x = 0.09$.

The comparison of the experimental Raman spectra with the one-phonon frequency distribution indicates that the most important part of the intrinsic scattering is of second-order nature; nevertheless, especially in the frequency range between 150 and 300 cm^{-1}, a possibility of a first-order contribution exists on the basis of our calculation. The weakness of these lines intensities and their specific dependences with niobium concentration and temperature seem to be in disfavor of the spin-glass model, in which the Nb ions are assumed off centered at norpressure and temperature, but are rather in agreement with the cooperative dynamic cluster description as proposed by Lyons et al.[17]

C. Calculation of the second-order Raman intensity

Figure 9 shows non-negligible differences between the thermally weighted two-phonon density and the experimental Raman spectrum. This fact proves the highly
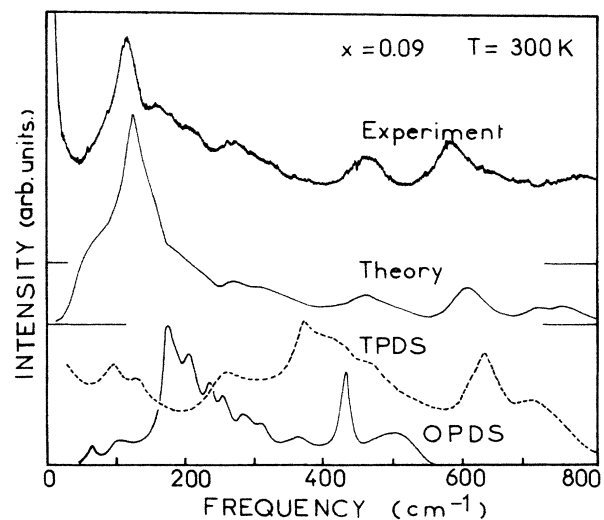

FIG. 9. Comparison between the experimental Raman spectrum, the one-phonon density of state (OPDS), and the thermally weighted two-phonon density of state (TPDS) calculated in $KTa_{1-x}Nb_xO_3$ ($x = 0.09$) at 300 K. The selective character of the polarizability tensor is show by the theoretical Raman curve.

selective character of the polarizability elements $P_{\alpha\beta}(^{q}_{j_1}$ $^{-q}_{j_2})$ in the scattering processes. By taking into consideration these coefficients, a good agreement between the calculated intensity and the experimental spectrum can be achieved, as reported in Fig. 9. The present section will deal with the detailed analysis of this aspect with respect to symmetry, niobium concentration, and temperature.

Figure 10 represents the symmetry component A_{1g} and E_g of the Raman spectrum calculated in the KTN crystal ($x = 2\%$) at room temperature. The frequencies of the obtained structures, their relative intensities within each spectrum, as well as their ratio according to the symmetry indicate a behavior comparable to the experimental spectrum. These results clearly point out that the nonlinear mechanisms involved in our calculations which were primarily at the origin of ferroelectric mode softening are also responsible for the intense second-order Raman scattering. The assignment which has been proposed in Fig. 1 is confirmed by our calculations.

A further valuable test of the model consists in the comparison between the theoretical and experimental profiles as a function of temperature and for the various concentrations of Nb in the crystals. For this purpose, we report in Fig. 11, 12, and 13 the theoretical Raman results for the main A_{1g} symmetry component at room and at low temperature for the crystals with $x = 0.008$, $x = 0.012$, and $x = 0.02$, respectively. The features which appear in the experiment, as, for example, the gradual lowering of the $2TA(X)$ peak and the disappearance at low temperature of the lines assigned due to difference processes, are accurately reproduced.

At low temperatures, the theoretical intensity curves exhibit on the low-frequency side of the main $2TA(X)$ peak an additional sharp and intense structure, appearing in the same frequency range as the broad experimental shoulder detected at temperatures slightly above T_c.
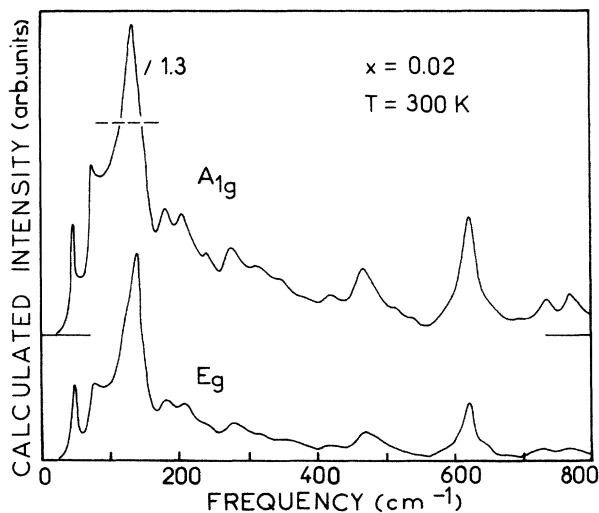

FIG. 11. Calculated Raman spectrum of symmetry A_{1g} in $KTa_{1-x}Nb_xO_3$ ($x - 0.008$) for two temperatures (300 and 30 K).

From our calculations this supplementary line can be assigned as due to combination processes involving the ferroelectric mode TO_1 and the transverse TA mode. This assumption is coherent with the temperature behavior of the soft mode measured by hyper-Raman spectroscopy.[9] The following question then arises: Why did the corresponding experimental line appear with a scattering profile showing a significant difference from the calculated one? One conceivable explanation originates in the strong damping possessed by the ferroelectric mode at temperatures in the vicinity of T_c. This overdamping may also influence the second-order scattering. Since this phenomenon is not included in our model, the calculation can not afford structure broadening due to individual phonon lifetime. Furthermore, on pure $KTaO_3$ (Refs. 38

FIG. 10. Second-order Raman spectrum calculated for the two irreducible A_{1g} and E_g components in $KTa_{1-x}Nb_xO_3$ ($x = 0.02$) at room temperature.

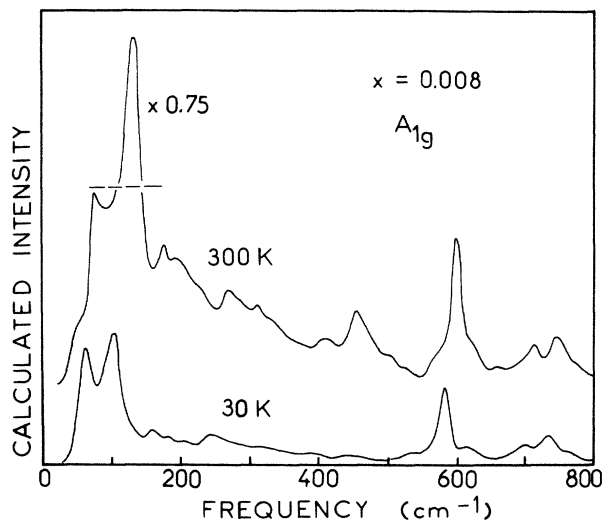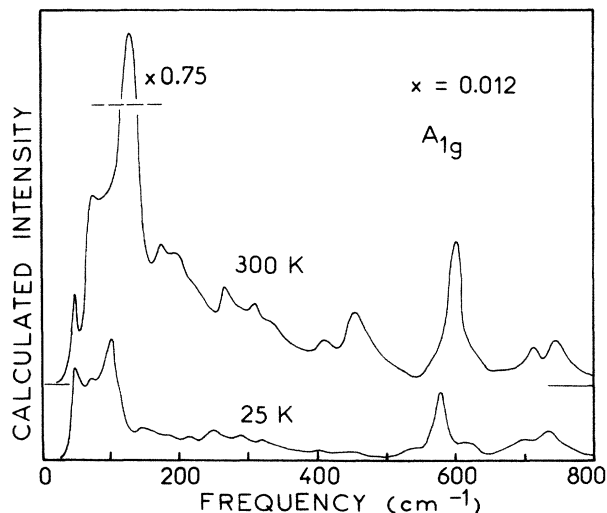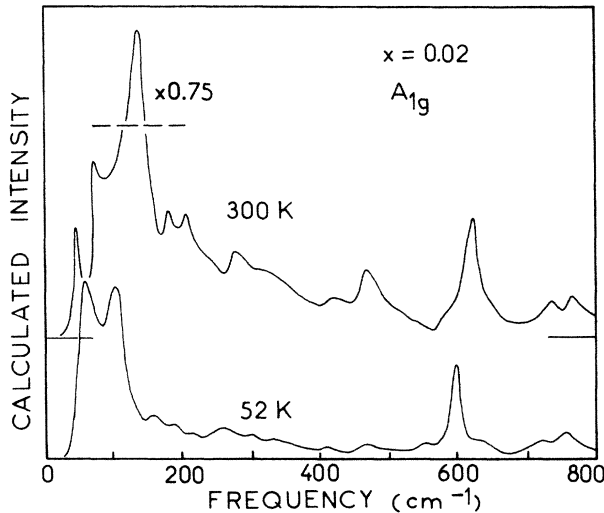FIG. 12. Calculated Raman spectrum of symmetry A_{1g} in $KTa_{1-x}Nb_xO_3$ ($x = 0.012$) for two temperatures (300 and 25 K).

FIG. 13. Calculated Raman spectrum of symmetry A_{1g} in $KTa_{1-x}Nb_xO_3$ ($x = 0.02$) for two temperatures (300 and 52 K).

and 39) as well as on KTN (Ref. 21) samples, inelastic neutron scattering measurements showed a strong and anomalous coupling between the optic TO_1 branch and the transverse TA branch for small but nonzero wave vectors q. These interactions may yield smearing out of the sharp structures, as observed on the experimental curve.

The comparison of the experimental Raman spectra of the various investigated KTN crystals at a given temperature, as, for example, room temperature, indicates the occurrence, in addition to the feature which has been already discussed, of a very broad quasielastic background increasing with increasing niobium concentration. These effects are not reproduced by our calculations. As proposed by Prater et al.[15] it is possible that they originate from supplementary excitations involving the Nb ions. Similar features comparable to strong tails of a central peak have been observed in other niobium compounds such as $AgNbO_3$ (Ref. 40), $NaNbO_3$ (Ref. 41), and $KNbO_3$ (Ref. 42). Although ordinary two-phonon difference scattering cannot be entirely excluded as a possible origin of this diffuse quasielastic scattering, its strong dependence on niobium concentration rather suggests a mechanism involving fluctuations due to disorder in the polarizabilities introduced by the Nb substitution.

A last major point, which should be noted in our low-temperature Raman scattering measurements, is the gradual appearance at temperatures slightly above the true critical temperature T_c of first-order lines characteristic of the low-temperature phase. These anomalous structures are particularly obvious for the KTN crystals with $x = 0.02$ at 35 K, where the Raman spectrum exhibits an additional low-frequency scattering similar to an overdamped soft-mode scattering as well as two small, but evident, lines at 200 and 548 cm^{-1} corresponding to the TO_2 and TO_4 phonons, respectively. Similar features are seen in KTN with $x = 0.008$ at 8 K. These observations will be discussed in a forthcoming paper. We only mention here that these precursor effects are coherent with the description of Höck and Thomas,[43] suggesting a freezing out of the impurities at a local temperature T_c^{loc} above the true critical temperature of the whole crystal.

V. CONCLUSIONS

A number of conclusions based on the experimental and theoretical study of the Raman spectra of KTN crystal in the paraelectric phase have been reached here. First, the Raman spectra for the KTN crystals, even for those with high niobium concentration, can be interpreted, for temperature T higher than $T_c + \Delta T$ (where ΔT is small temperature range depending on the Nb concentration) by second-order processes involving mainly the critical X point of the Brillouin zone. Second, the nonlinear electron-ion coupling in the highly polarizable oxygen ion, which has been found to be at the origin of the ferroelectric mode softening, is primarily responsible for the strong second-order Raman spectra. Introduction of niobium ions in $KTaO_3$ yields an enhancement of these nonlinear polarizabilities which favors a stabilization of a low-temperature ferroelectric phase. Third, since no disorder-induced scattering is observed, the Nb impurities are assumed to be in on-center position at temperatures far enough from the true critical temperature. This result has been ascertained recently by van der Klink et al.[44] by NMR measurements. In the near vicinity of T_c below a local critical temperature T_c^{loc} and due to the incipient instability allowed by the anharmonic polarizability, the niobium ions freeze-out, leading to polarization fluctuations and clusters which enable an important quasielastic scattering and occurrence of precursor first-order scattering.

[1]K. A. Müller and H. Thomas, in *Structural Phase Transitions* Vol. 23 of *Current Topics in Physics* (Spinger, Berlin, 1981).

[2]H. Z. Cummins and A. P. Levanyuk, *Modern Problems in Condensed Matter Sciences* (North-Holland, Amsterdam, 1983), Vol. 1.

[3]M. E. Lines and A. M. Glass, *Principes and Applications of Ferroelectrics and Related Materials* (Clarendon, Oxford, 1977).

[4]H. Vogt and H. Uwe, Phys. Rev. B **29**, 1030 (1984).

[5]S. K. Kurtz, Bell Syst. Tech. J. **45**, 1209 (1966).

[6]L. A. Boatner, U. T. Höchli, and H. E. Weibel, Helv. Phys. Acta **50**, 620 (1977).

[7]D. Rytz, U. T. Höchli, and H. Bilz, Phys. Rev. B **22**, 359 (1980).

[8]D. Rytz, Ph.D. thesis, Ecole Polytechnique Fédérale de Lausanne, 1983.

[9]G. Kugel, H. Vogt, W. Kress, and D. Rytz, Phys. Rev. B **30**,

985 (1984).

[10] M. Dubus, D. Baudin, B. Salce, and L. A. Boatner, Solid State Commun. **55**, 759 (1985).

[11] E. Lee, L. L. Chase, and L. A. Boatner, Phys. Rev. B **31**, 1438 (1985).

[12] G. A. Samara, Phys. Rev. Lett. **53**, 298 (1984).

[13] W. Kleemann, F. J. Schäfer, and D. Rytz, Phys. Rev. Lett. **54**, 2038 (1985).

[14] B. I. Halperin and C. M. Varma, Phys. Rev. B **14**, 4030 (1976).

[15] R. L. Prater, L. L. Chase, and L. A. Boatner, Phys. Rev. B **23**, 221 (1981).

[16] Y. Yacoby, Z. Phys. B **31**, (1978).

[17] K. B. Lyons, P. A. Fleury, and D. Rytz, Phys. Rev. Lett. **57**, 2207 (1986).

[18] D. Rytz, M. D. Fontana, J. L. Servoin, and F. Gervais Phys. Rev. B **28**, 6041 (1983).

[19] R. Currat, H. Buhay, C. H. Perry, J. D. Axe, W. G. Stirling, and R. P. Lowndes (unpublished).

[20] W. B. Yelon, W. Cochran, G. Shirane, and A. Linz, Ferroelectrics **2**, 261 (1971).

[21] M. D. Fontana, W. Kress, G. Kugel, N. Lehner, and D. Rytz, Ferroelectrics **55**, 23 (1984).

[22] G. E. Kugel, M. D. Fontana, and W. Kress, Phys. Rev. B **35**, 813 (1987).

[23] G. E. Kugel, M. D. Fontana and W. Kress, Jpn. J. Appl. Phys., Suppl. 24-2 **24**, 220 (1985).

[24] D. Rytz and H. I. Scheel, J. Cryst. Growth **59**, 468 (1982).

[25] L. T. Todd, Masters thesis, MIT, 1969.

[26] W. G. Nilsen and J. G. Skinner, J. Chem. Phys. **47**, 1413 (1967).

[27] R. Migoni, H. Bilz, and D. Bäuerle, Phys. Rev. Lett. **37**, 1155 (1976).

[28] R. Migoni, H. Bilz, and D. Bäuerle, in *Lattice Dynamics*, edited by M. Balkanski (Flammarion, Paris, 1978), p. 650.

[29] W. G. Nilsen and J. G. Skinner, J. Chem. Phys. **48**, 2240 (1968).

[30] K. H. Rieder, B. A. Weinstein, M. Cardona, and H. Bilz, Phys. Rev. B **8**, 4780 (1973).

[31] R. Loudon, Adv. Phys. **13**, 423 (1964).

[32] A. D. Bruce and R. A. Cowley, J. Phys. C **5**, 595 (1972).

[33] R. Haberkorn, M. Buchanan, and H. Bilz, Solid State Commun. **12**, 681 (1973).

[34] H. Bilz, M. Buchanan, K. Fischer, R. Haberkorn, and U. Schröder, Solid State Commun. **16**, 1023 (1975).

[35] R. A. Cowley, Phys. Rev. **134**, A981 (1964).

[36] W. Stirling, J. Phys. C **5**, 2711 (1972).

[37] R. Migoni, thesis, Universität of Stuttgart, 1976.

[38] J. D. Axe, J. Harada, and G. Shirane, Phys. Rev. B **1**, 1227 (1970).

[39] R. Comes and G. Shirane, Phys. Rev. B **5**, 1886 (1972).

[40] A. Kania, K. Roleder, G. E. Kugel, and M. D. Fontana, J. Phys. C **19**, 9 (1986).

[41] F. Denoyer, M. Lambert, R. Comes, and R. Currat, Solid State Commun. **18**, 441 (1976).

[42] M. D. Fontana and G. E. Kugel, Jpn. J. Appl. Phys., Suppl. 24-2 **24**, 223 (1985).

[43] K. H. Höck and H. Thomas, Z. Phys. B **27**, 267 (1977).

[44] J. J. van der Klink, S. Rod, and A. Châtelain, Phys. Rev. B **33**, 2084 (1986).